On the Microstructure of Off-Eutectic Au-Ge Joints: A High-Temperature Joint

Larsson, Andreas[1, 2]; Aasmundtveit, Knut[2]
[1]Techni AS - Techni AS
[2]Institutt for mikrosystemer - Universitetet i Sørøst-Norge

This is the accepted version of an article published in *Metallurgical and Materials Transactions A*. The final authenticated version is available online at:
https://doi.org/10.1007/s11661-019-05530-4

Publisher's version: Larsson, A. & Aamundtveit, K. E. (2020). On the Microstructure of Off-Eutectic Au-Ge Joints: A High-Temperature Joint. *Metallurgical and Materials Transactions A, 51*(2), 740-749.
https://doi.org/10.1007/s11661-019-05530-4

On the microstructure of off-eutectic Au–Ge joints — A high-temperature joint

ANDREAS LARSSON
ANDREAS LARSSON is at TECHNI AS Dep. of applied physics, Borre, Norway and University of South-Eastern Norway (USN), Dep. of materials and micro-integration, Borre, Norway. Contact e-mail: andreas.larsson@techni.no; ala@usn.no

KNUT E. AAMUNDTVEIT
KNUT E. AAMUNDTVEIT is at the University of South-Eastern Norway (USN), Dep. of materials and micro-integration, Borre, Norway. Contact e-mail: knut.aasmundtveit@usn.no

ABSTRACT

Joining delicate electronic components for high-temperature applications is challenging. Regular soldering with lead-free or lead-based materials is typically not suitable for high-temperature applications due to their low melting points. Using off-eutectic compounds for joints offer an easy and gentle process creating joints that can be formed at a lower process temperature than the final operation temperature. Microstructural evolution near the eutectic melting point is key to be able to form reliable joints. A layered Au / eutectic Au–Ge / Au structure was used to form Au-rich off-eutectic Au–Ge joints. Columnar-like structures of primary α-phase (Au) protruded through a Ge rich off-eutectic Au–Ge mixture at the center of the joint. These structures connect the joined pieces with a single solid phase with a melting point of *ca.* 1064 °C. The microstructure coarsened when exposed to temperatures between (300–380) °C, *i.e.,* near the eutectic melting point at 361 °C. Ge diffused and accumulated along grain boundaries between Au grains. Annealing above the eutectic melting point, Ge rapidly diffused and formed larger colonies of pure Ge surrounded by a Au matrix. This accords well with our previously published results demonstrating shear strength capacity of similar joints at temperatures well above the eutectic temperature.

Keywords—Au–Ge, joining, bonding, high temperature, Off-eutectic microstructure

I. INTRODUCTION

Many industries and applications require high-temperature compatible electronic systems, including down-hole instrumentation in oil, gas, and geothermal wells, power electronics in automotive (electric vehicle (EV) and hybrid electric vehicle (HEV)), and thermoelectric energy harvesting. In recent years many high-temperature compatible components have been developed and demonstrated. Devices made from wide-bandgap materials have been demonstrated to operate at high temperatures[1]. In particular, silicon carbide (SiC) and gallium nitride (GaN), have demonstrated their potential in commercial devices[2]. They offer high-temperature stability with low losses due to fast switching speeds. This reduces the need for costly and bulky cooling systems[1]. To enable the integration of high-temperature compatible components into electronic systems require high-temperature stable joints. Joints formed with a process temperature that is lower than the final operation temperature of the joints have been evaluated for high-temperature applications. Such joining technologies include transient liquid phase (TLP) bonding[3–7], solid-liquid interdiffusion (SLID) bonding[8–10], and sintering[11–13]. TLP, SLID and sintering are often limited by long process times or require a high bond line pressure during fabrication. Another joining technology that can be used with high-temperature compatible devices is soldering, which require relatively high process temperatures. Unlike TLP, SLID, and sintering, soldering is typically quick with limited requirement for applied bond line pressure.

Eutectic gold (Au) based joints are a feasible option for high-temperature applications up to around 300 °C[14–16], e.g. gold–silicon (Au–Si, eutectic temperature at 363 °C[17]), gold–germanium (Au–Ge, eutectic temperature at 361 °C[18]), and gold–indium (Au–In, eutectic temperature at 450–496 °C[19]). In a recent study, we have demonstrated that Au-rich off-eutectic Au–Ge joints have significant shear strength capacity, (39 ± 9) MPa at 410 °C[20], *i.e.,* 50 °C above the eutectic temperature at 361 °C. In other studies, we have demonstrated an increased effective melting point, > 600 °C, of similar Au-rich Au–Ge joints[21–23]. These joints seem to have the same benefits as regular eutectic joints, *i.e.,* fast and low bond line pressure while sharing the attractive feature of TLP, SLID and sintering, offering a lower process temperature than the final operation temperature. For off-eutectic

joints to be used near, or above the eutectic melting point, it is crucial that the kinetics of microstructure is stable or predictable. This study focuses on the microstructure and its evolution when exposed to high temperatures close to the eutectic melting point.

The bonds in this study are made by sandwiching a eutectic Au–Ge preform between Au layers, being an adequate bonding method for die-attach applications. To be able to study the microstructural evolution of the joint itself, the dies and substrates were omitted from the system. Instead, Au films were joined together with eutectic Au–Ge preforms, providing a model system for a die-attach bond without the potentially complicating factor of interdiffusion of joint components with adjoined materials.

The results show that a Au-rich off-eutectic mixture was formed. Structures of primary Au protrude through a Ge-rich off-eutectic Au–Ge layer at the original bond line. Annealing near or above the eutectic melting point drive diffusion of Ge to accumulate into larger colonies located at grain boundaries between Au grains.

II. MATERIALS AND METHODS

A. *Materials and fabrication*

Eutectic Au–Ge preforms were sandwiched between foils of pure Au to create off-eutectic Au–Ge joints. The Au foils were manufactured by electroplating on Si substrates and detached by mechanical lift-off. The Au thickness was 22 ± 2 µm. Pieces of a slightly smaller size than the Au foils, but with the same shape as the Au foil pieces were cut manually from a eutectic Au–Ge preform, *i.e.,* $Au_{72}Ge_{28}$, (Goodfellow). The preform was 35 ± 2 µm thick, and the Ge concentration in the preform was between 28–39 at.%. Two pieces of the Au foil and one piece of eutectic preform were adjoined on a hot plate to form a symmetrical Au / Au–Ge / Au structure. 60 ± 0.5 µm thick spacers were placed on opposite sides of the materials stack. A bridge made from a piece of Si wafer (525 ± 25 µm) was placed over the spacers and material stack, and a clamp was used to apply a force (~9 N) on the stack to facilitate a thermomechanical contact between the metallic pieces. The configuration is shown in Fig. 1. The spacers enable fabrication of joints with a uniform and constant thickness. It also enables bonding with a very low bond line pressure after melting of the preform. Although an increase in bond line pressure is expected during solidification since eutectic Au–Ge expands by about 5% when it solidifies[24]. The overall Ge concentration of the fabricated joints was 6.9 ± 1.9 at.% Ge. This Au rich, hypoeutectic, composition is marked with a dashed region, c_0, in the binary Au–Ge phase diagram depicted in Fig. 2. The assembly was put into a vacuum chamber, and the air was evacuated to a chamber pressure of 1-10 mTorr. The hot plate temperature was raised to melt the preform. A characteristic temperature profile is shown in Fig. 3. Annealing was performed by placing samples into a vacuum bonder (Budatec VS160UG). The annealing was carried out in a vacuum, 1 mTorr, and a temperature close to the melting point, 330 °C. This equals a homologous temperature of 0.95, where the diffusivity is as high as possible without being too close to the melting point where more rapid liquid diffusion must be considered. Samples were annealed for 1, 4, 16, 24, 52, and 70 hours and examined to evaluate the evolution of the microstructure. Samples were also annealed at 300 °C for 144 hours in dry nitrogen at 1 atm. A thermal cycle regime was used to study microstructural evolution caused by partial melting. Samples were heated up to 380 °C, *i.e.* ~20 °C above the eutectic melting point, at a rate of ~15 °C/min and then cooled down to room temperature at a rate of ~22 °C/min.

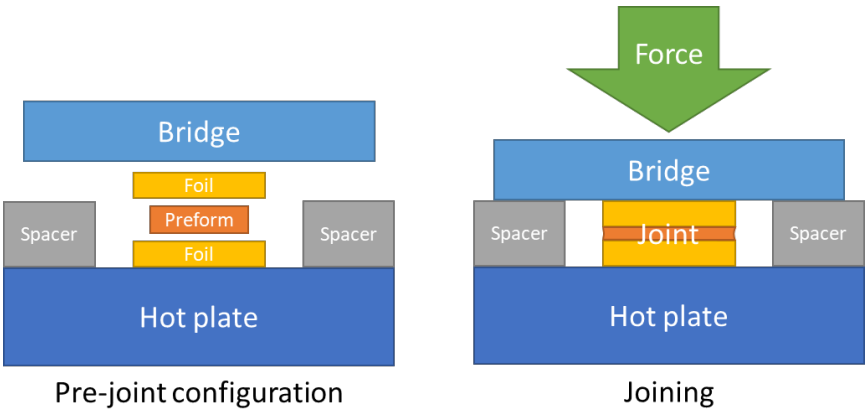

Fig. 1. Schematic figure of the configuration used to fabricate off-eutectic Au–Ge joints. One piece of eutectic preform foil is sandwiched between pieces of Au foils. Two spacers are placed on opposite sides of the material stack, and a bridge and clamp are used to press the components together on the hot plate.

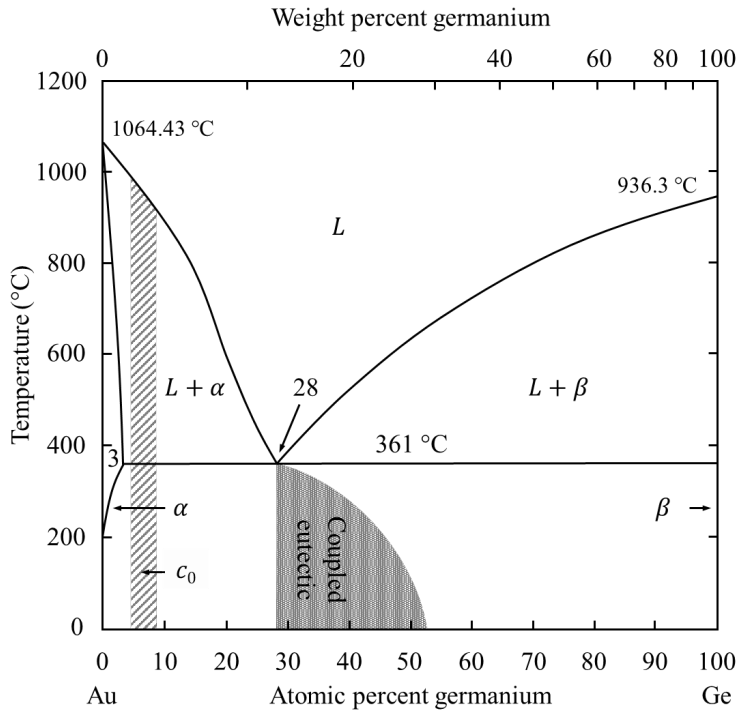

Fig. 2. Illustration of the binary phase diagram of the Au–Ge system. The target Au rich off-eutectic composition, c_0, of the fabricated joints is marked with a dashed region. The phase diagram was adapted from Okamoto and Massalski[18]. Note that the eutectic melting point varies slightly in the pertinent literature; 356-361 °C [25,26]. NB, the coupled eutectic zone (shaded region) is for illustrative purposes only.

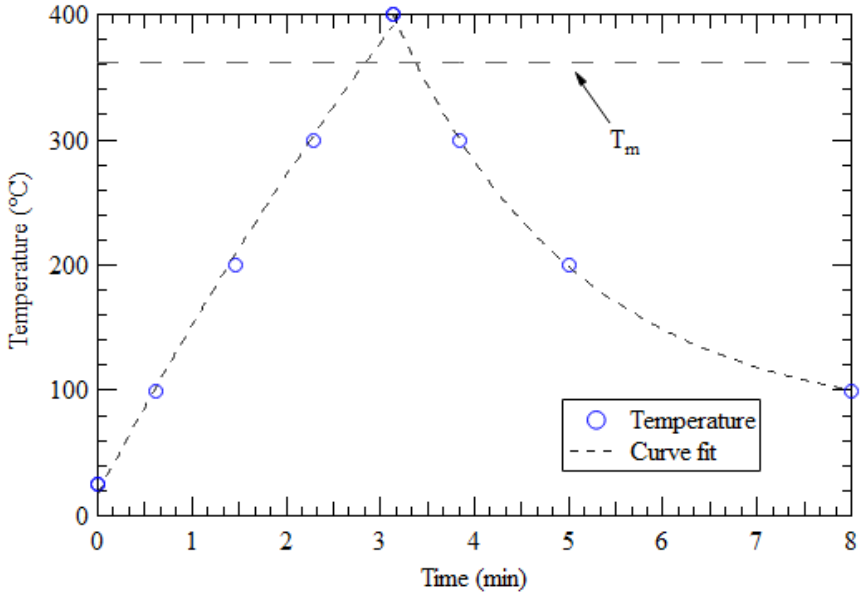

Fig. 3 Temperature profile used during bonding to fabricate virgin samples. Samples are heated with a constant rate of 120 °C/min up to 400 °C in a vacuum, 1-10 mTorr. A passive cooling stage is then initiated. The sample is exposed to a temperature above the eutectic melting point for 30-40 seconds before solidification occurs at a cooling rate of roughly 140-160 °C/min. The eutectic melting point, T_m, is marked with a dashed line.

B. *Characterization*

The microstructure was studied by investigation of cross-sections from the fabricated samples. Cross-sections were prepared in two planes through the samples, perpendicular, ⊥, or parallel, ∥, to the bond line plane, see Fig. 4. Samples set for ⊥-plane cross-section analysis were prepared by ion-milling (Hitachi IM4000, Ar) in cross-section mode creating fresh surfaces. Samples set for ∥-plane cross-section analysis were prepared by grinding and

polishing, finished by flat ion milling. The grinding stopped at 2000 or 4000 grit grade before preparation was continued with polishing using a cloth and a 1 µm diamond paste for the final step. Then the samples were finished with flat ion milling (Hitachi IM4000, Ar). Optical microscopy (Neophot 32, NA 0.9, up to 1000x magnification) provided color information for phase recognition and evaluation of morphology. Scanning electron microscopy (SEM) (Hitachi SU8230) was used for a more detailed examination of the microstructure. The composition and morphology were evaluated by energy-dispersive X-ray spectroscopy (EDX) (Oxford X-MAX 150), and electron backscattered diffraction (EBSD) (Oxford NordlysMax^3).

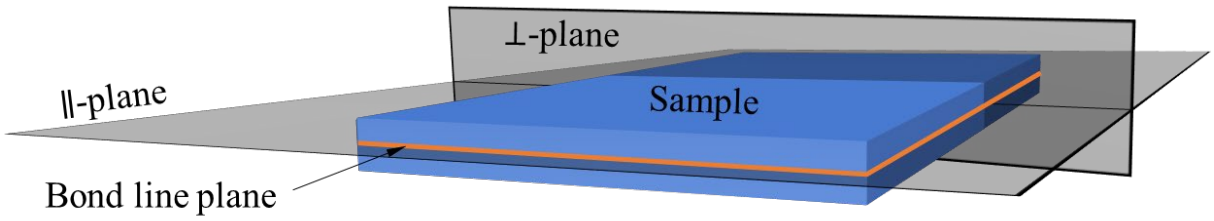

Fig. 4. Illustration of the definition of notation of planes for cross-sections.

III. RESULTS AND DISCUSSION

A. *Microstructure*

Cross-sections showed joints of high quality with very few voids or cracks. The joints consisted of a layer of eutectic Au–Ge compound between Au layers. This eutectic Au–Ge compound was not uniformly distributed in the bond line, as can be clearly seen in Fig. 5, showing the EDX map of Ge distribution in a ∥-plane cross-section located approximately at the center of the bond line. This inhomogeneity can also be clearly seen in the three different cross-sections (⊥-plane) in Fig. 6. Fig. 6(a) show a continuous band of eutectic Au–Ge between the Au layers, whereas Fig. 6(b)-(c) show isolated colonies of eutectic Au–Ge adjacent to areas where the bond line is a continuous Au structure. In Fig. 6(c) the microstructure is close to being monometallic Au, with only small regions of eutectic Au–Ge. In the most extreme case, mm long sections were found that were completely without any detectable Ge, visually or by EDX. A joint with a microstructure similar to Fig. 6(a) throughout the entire joint, *i.e.,* with a continuous layer of eutectic Au–Ge between Au layers, would form a liquid interlayer between the Au layers upon remelting at the eutectic melting point of 361 °C. A microstructure like the one shown Fig. 6(b)-(c) would remelt at 361 °C locally near the Au–Ge colonies, while the remaining section would remelt at a significantly higher temperature due to the continuous Au structures throughout the joint. A structure as shown in fig. 6c suggests that the remelting temperature might be as high as the melting point of primary Au (up to 1064 °C). Fig. 7(a) shows a ∥-plane cross-section where large Au domains are surrounded by a mixture with a eutectic Au–Ge microstructure (detailed view in Fig. 7(b)). Combining the results from the both the ⊥-plane and ∥-plane cross-sections depicts a microstructure where columnar structures of Au extend through an interlayer of eutectic Au–Ge at the bond line plane, as illustrated in Fig. 8. Fig. 9 shows a fracture surface of a similar off-eutectic Au–Ge joint that was shear tested at 370 °C, *i.e.* above the eutectic melting point, in another study[20]. The fracture surface show a similar microstructure as can be seen in Fig. 7 and illustrated in Fig. 8, *i.e.* solid columnar structures protruding through the joint. These columnar structures explains the remarkable high-temperature shear strength capacity at temperatures above the eutectic melting point. The shear strength was quantified to be around 40 MPa at temperatures around 400 °C for a similar Au–Ge joint as shown in Fig. 10[20]. The measured high-temeprature shear strength is ten times higher than the room temperature requirement in MIL-STD-883H[27], and roughly twice as high as the room temperature shear strength of regular Sn–Pb and SAC joints.

The preforms used to fabricate samples had an overall uniform and homogeneous microstructure before joining, as can be seen in Fig. 11. This means that the layered foil / preform / foil structure was uniform and laterally homogeneous before joining. Joining transforms this structure into a new microstructure where the middle (preform) layer lose its homogeneity as it reacts with the adjoining layers. When the preform melts, rapid solid-liquid interdiffusion between the melt and the adjoining Au layers create a period of dissolution (melt back) of Au into the layer expanding the melt, *i.e.,* the volume of the liquid phase increase[7]. This changes the composition of the melt into a hypoeutectic composition with a composition defined by the liquidus, and the concentration of the solid Au surface will have a concentration according to the solidus[6]. The joint transition into the two-phase field region ($L + \alpha$) initiating the solidification process[6]. Nucleation and crystal growth of the primary Au phase begins to form in the melt[28–30]. Note that complete isothermal solidification cannot be accomplished (*cf.* the transient liquid phase (TLP) process[6,7]) since there is not enough Au in the system to form a solid homogeneous α-phase, *i.e.,* the Ge concentration is too high; >3 at.%. When the temperature is reduced below the eutectic isotherm, the

remaining liquid phase solidifies into the α-phase and a eutectic mixture[28,29]. A few spherical voids were seen in the bond line, as seen in fig. 6a). They were likely formed by trapped gas during joining[31].

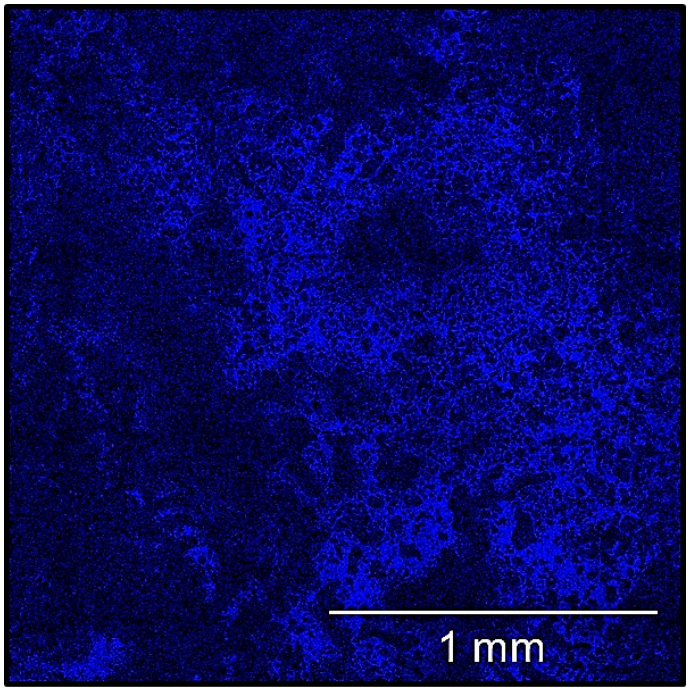

Fig. 5. EDX map (20 keV) of Ge (blue) in a ∥-plane cross-section approximately at the original bond line (joint center) of a virgin sample showing an inhomogeneous Ge distribution in the joint.

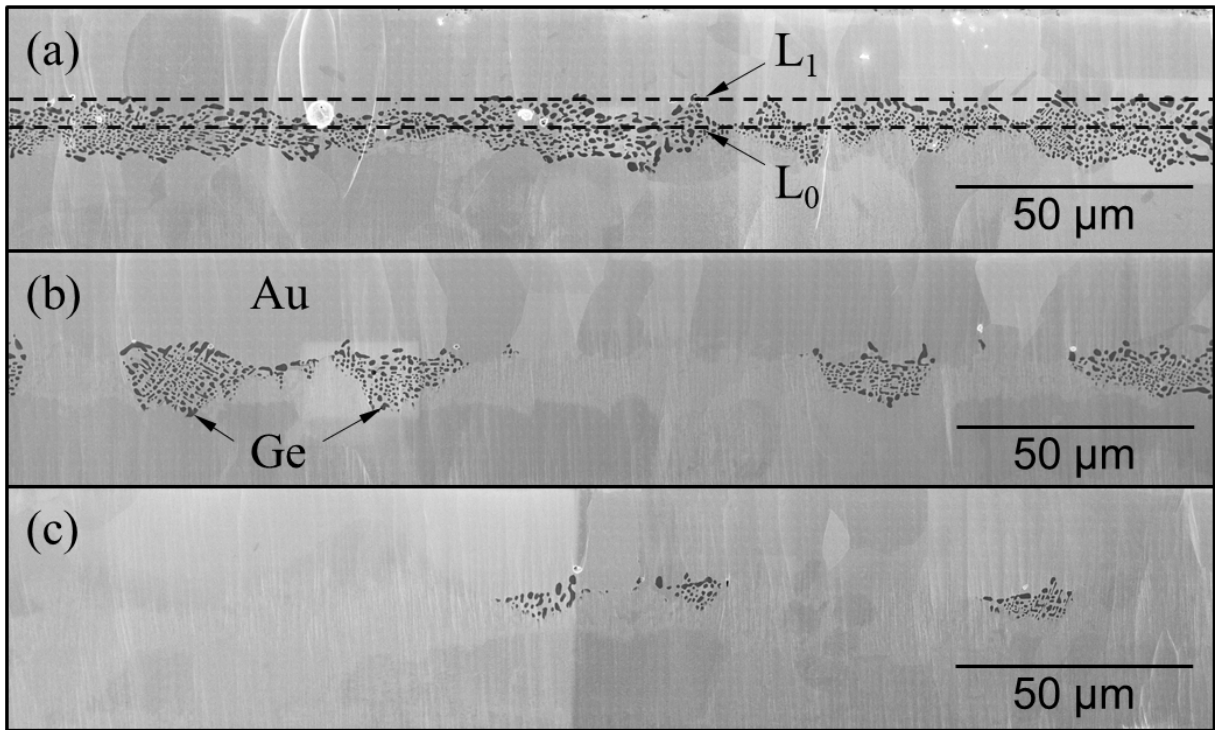

Fig. 6. Three sections from different parts of the same cross-section (⊥-plane) of the same sample illustrating the inhomogeneous microstructure of the fabricated Au rich off-eutectic Au–Ge joints. (a) Shows a band of eutectic Au–Ge structures at the center of the joint, *i.e.,* at the original bond line. The dashed lines L_0 and L_1 are equivalent locations of ∥-plane cross-sections, as shown in Fig. 7(a), and Fig. 18. (b) shows colonies of eutectic Au–Ge surrounded by Au (α-phase). (c) shows a section comprising also only the α-phase, with only small colonies of eutectic Au–Ge.

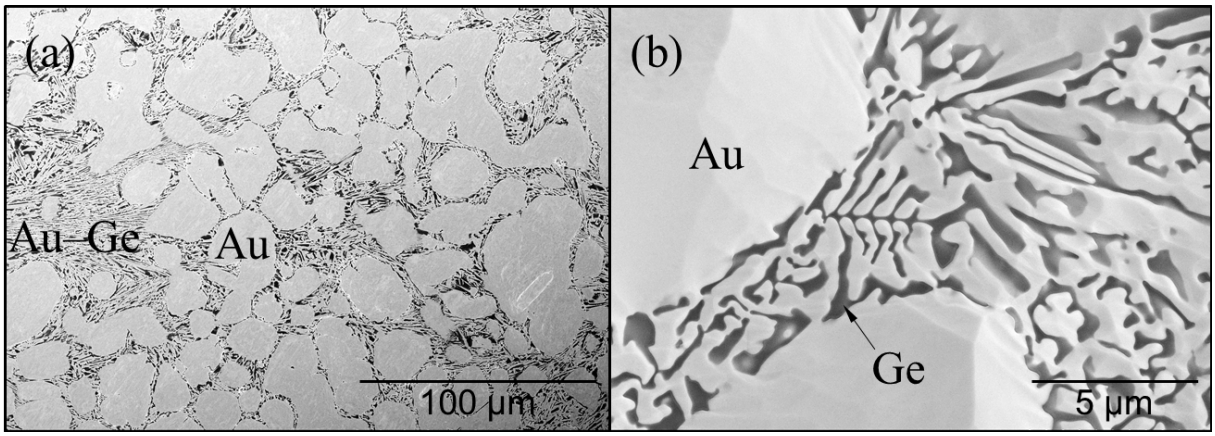

164

165 Fig. 7. SEM micrographs of in-plane cross-sections (‖-plane) of a virgin sample. (a) Shows an inhomogeneous
166 structure with Au precipitates surrounded by a Ge-rich eutectic mixture. The cross-section location is
167 approximately equivalent to L_0 in Fig. 6(a). (b) shows a magnified micrograph of a eutectic Au–Ge lamellae type
168 structure.

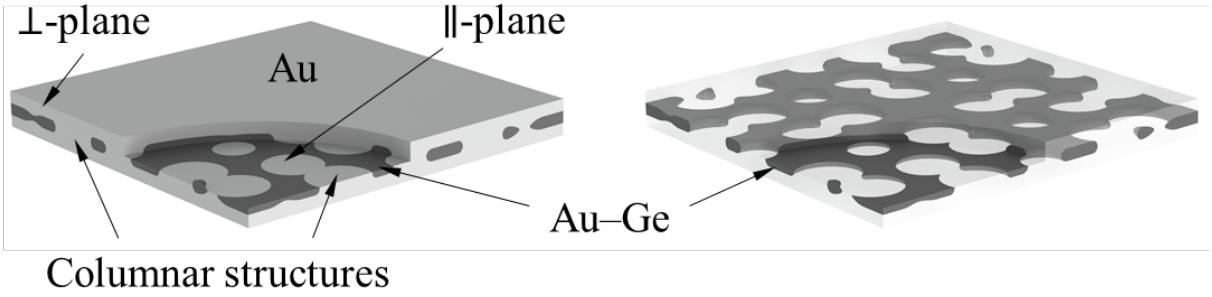

169

170 Fig. 8. 3D illustration of how the Au-phase (light) and the Au–Ge mixture (dark) are distributed inside the
171 fabricated joints. Columnar-like structures of Au extend through the eutectic Au–Ge layer. The Au-phase has been
172 made semi-transparent in the image to the right to provide a better view of the eutectic Au–Ge mixture.

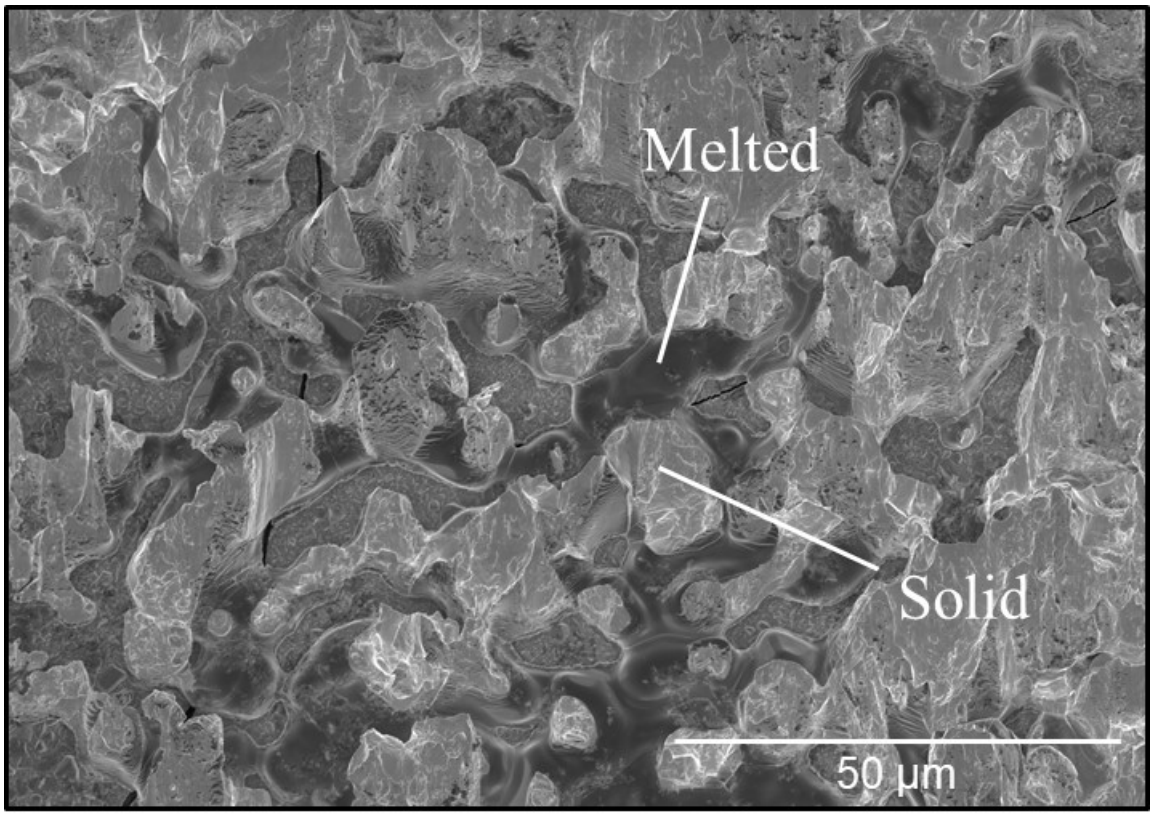

Fig. 9. SEM micrograph of fracture surface a off-eutectic Au–Ge joint sheartested at 370 °C, *i.e.* above the eutectic melting point. Columnar structures (solid) are surrounded by a phase that have apparently been in a liquid state (melted). These columnar structures show similatrities with the columnar structures illustrated in Fig. 8. Reprinted with permission[20].

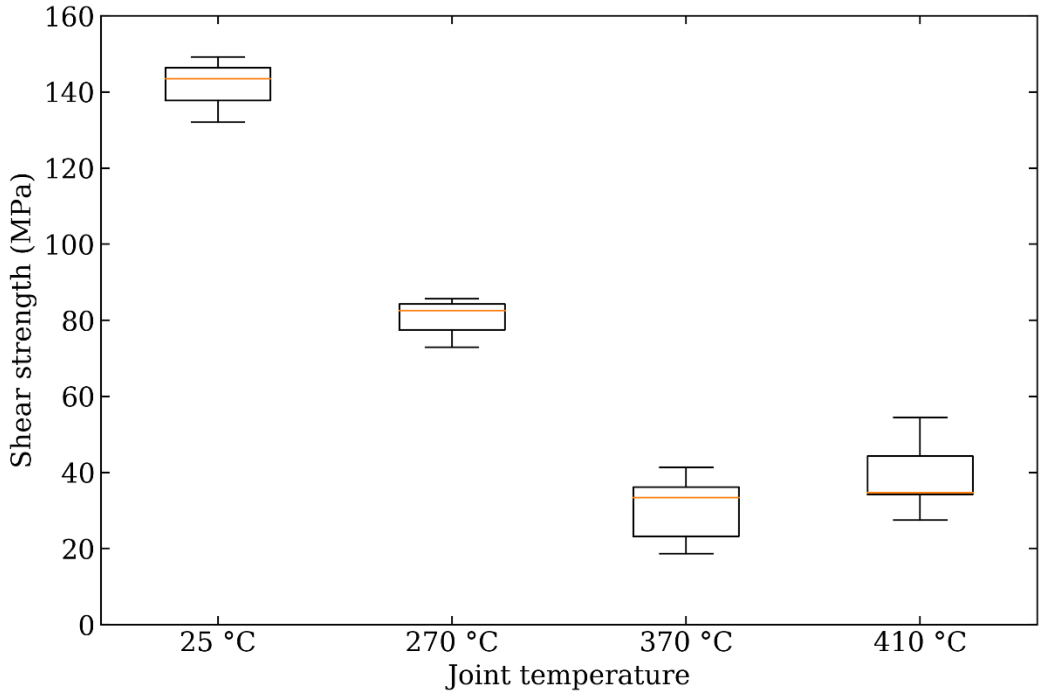

Fig. 10. Shear strength as a function of joint temperature. Reprinted with permission[20].

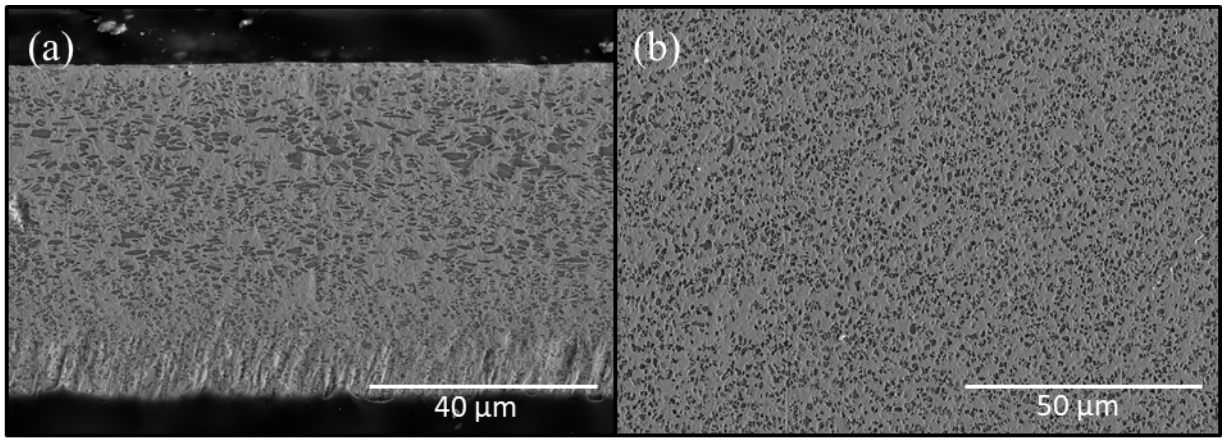

Fig. 11. SEM micrographs of the preform used to fabricated samples showing an overall uniform and homogeneous microstructure. (a) A ⊥-plane cross-section. (b) A ‖-plane cross-section.

B. *Composition*

The Au phase was measured by EDX to contain up to close to 3 at.% Ge. Thus, it is considered to be the primary α-phase in the Au–Ge system (Fig. 2). The Au–Ge mixture was measured to typically comprise a Ge-rich off-eutectic composition with up to roughly 50 at.% Ge, *i.e.,* a hypereutectic composition. This indicates that there is a coupled eutectic zone in the phase diagram for the growth rate impeded by the cooling rate used to fabricate samples[30,32,33]. The same hypereutectic composition range was also observed in the eutectic microstructure in annealed samples. This coupled eutectic zone is indicated with a shaded region in Fig. 2. The zone may have a different shape than shown here and is included for illustrative purposes only. This study was not intended to disclose such features, and no further investigations on this coupled zone were performed in this study. The Au and Ge phases exhibit clear contrast, both using SEM (SE-upper, SE-lower, and BSE detectors) and optical microscope as illustrated in Fig. 12. Despite this, intuitive interpretations of compositions in micrographs are difficult. Fig. 13 shows two sections with different microstructures that have the same Ge concentrations, 11.5 ± 0.6 at.% (3σ), present in the visible sections. Both sections were analyzed with an acceleration voltage of 15 kV exciting K and L-band electrons within an interaction volume of approximately 100 nm and 300 nm in Au and Ge respectively.

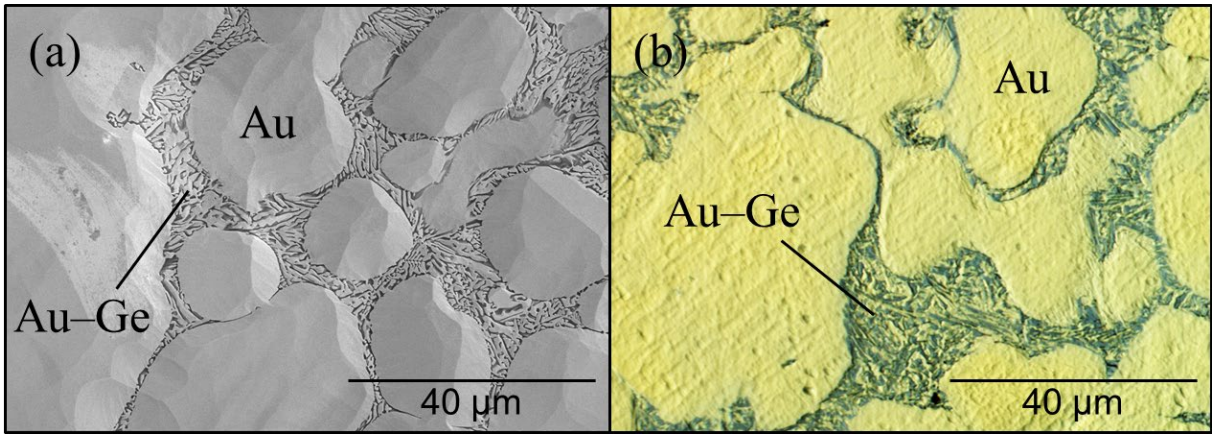

Fig. 12. ‖-plane cross-sections of the microstructure of virgin samples. (a) A SEM micrograph composed by images from both the upper and lower SE detectors combined into one image demonstrating a clear contrast between the light grey Au (α) phase and the dark grey Ge (β) phase. (b) Shows an optical micrograph, again demonstrating the clear contrast between the yellow Au (α) phase and the dark grey/green Ge (β) phase visible in the eutectic microstructure.

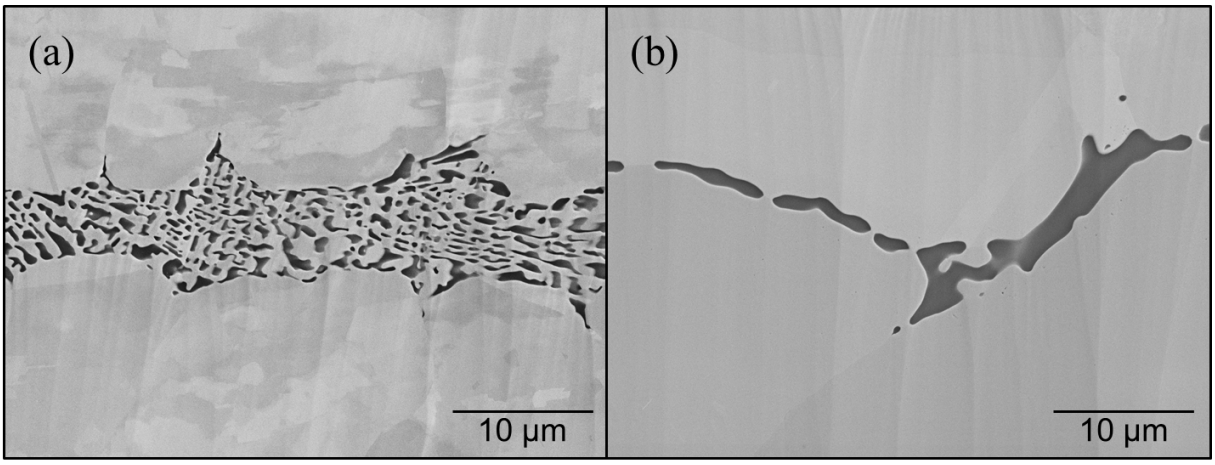

Fig. 13. SEM micrographs of two cross-sections (⊥-plane), with different microstructures, but with the same Ge concentration (11.5 ± 0.6 at.%) in the visible sections and captured with the same microscope settings at the same magnification. (a) Virgin sample. (b) A sample that has been partially melted.

C. *Microstructure evolution*

Annealed samples showed increased grain size and coarsened lamellae structure, as would be expected. This is particularly clear for the Ge domains which grow with time and temperature as can be seen in Fig. 14(a)-(d). An estimate of the average lamellar spacing as a function of annealing time at 330 °C is shown in Fig. 15. Fig. 16 shows a cross-section of a surface after 52 and 70 hours at 330 °C. One can see small changes in the shape of the Ge domains, showing an ongoing diffusion process. Fig. 14(e) shows a section that has been annealed at a slightly lower temperature of 300 °C for 144 h. Comparing it with a sample annealed at 330 °C for 70 hours (Fig. 14(d)), *i.e.,* approximately half the time, one can see that the coarsening have progressed further in the 330 °C, 70-hour sample. Exposing the samples to a temperature slightly above the eutectic melting point rapidly accelerates diffusion. Fig. 14(f) shows a section of a sample that has been cycled twice up to approximately 380 °C, *i.e.,* ~20 °C above the eutectic melting point at 361 °C, spending about 20 min in a partially liquid state. It is clear that the microstructure rapidly transforms when the temperature goes above the eutectic melting point. The typical eutectic microstructure, with a clear lamellae structure, is transformed into a microstructure comprising Au (α-phase) with large Ge (β-phase) domains. The Ge phase is located at the grain boundaries between Au grains. Fig. 17 shows the surface of a section before (virgin) and after exposure to a temperature (380 °C) above the eutectic melting point. It is clear from the surface topology that the material has been in a liquid state, see Fig. 17(b). Partial melting has also been confirmed by electrical characterization of the samples in another study[23]. Comparing ∥-plane cross-sections of virgin (Fig. 7(a)) and annealed (Fig. 18(a)) samples shows that the columnar Au structures appear to have a larger characteristic size in the annealed sample. The diameter has roughly doubled in size. Ge was found between the Au grains comprising the columnar structures. The Ge concentration was higher along the periphery of the structures than in the center region. It is still unclear why this is so. Ge may have diffused from the eutectic mixture surrounding the structures, along grain boundaries, and into the structures. Another alternative is that, as the Au structures grow, the Ge phase is pushed outward towards the periphery caused by phase segregation. The results suggest that Ge phase diffuses and accumulates into larger colonies or well-defined domains, always located at grain boundaries between Au grains, preferably at triple points.

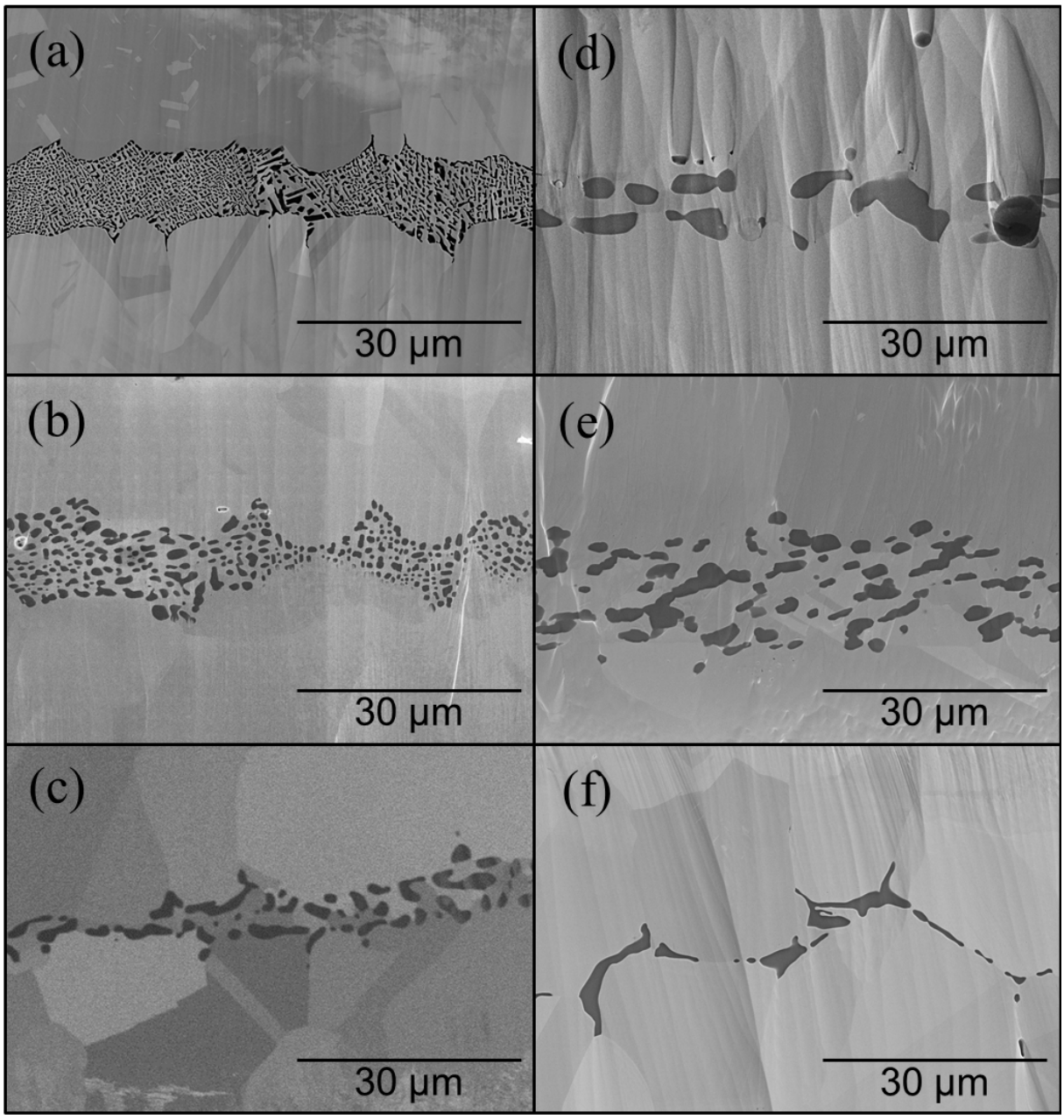

Fig. 14. SEM micrographs of cross-sections (⊥-plane) with a band of Ge domains in the center of the bond line from six samples exposed to different aging regimes: (a) Virgin, (b) 1 hour at 330 °C in vacuum, (c) 24 hours at 330 °C in vacuum, (d) 70 hours at 330 °C in vacuum, (e) 144 hours at 300 °C in nitrogen, (f) Cycled twice to 380 °C in air. The vertical stripes visible in cross-sections are artifacts created during sample preparation with ion-milling.

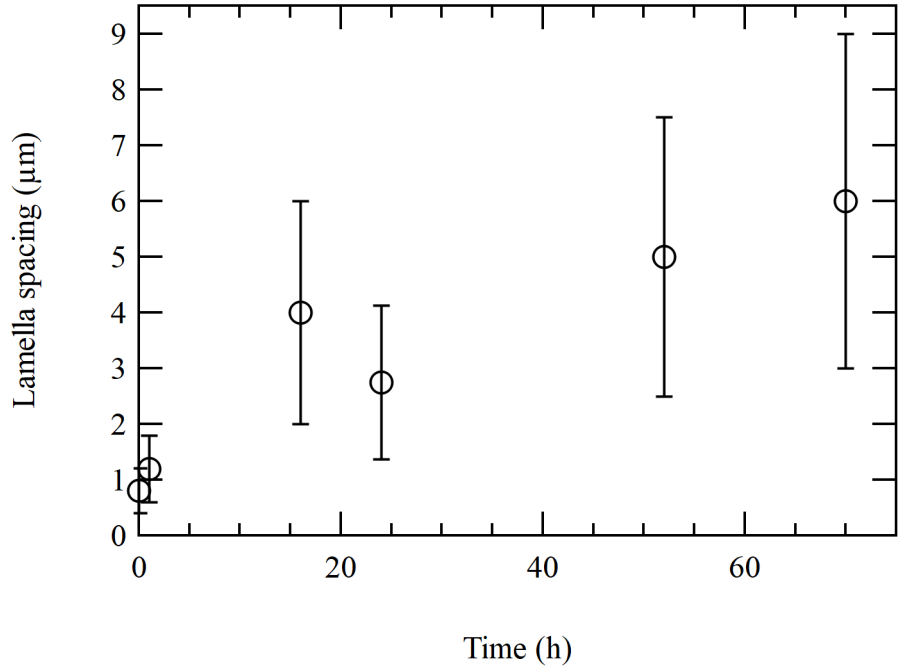

Fig. 15. Average lamellar spacing in eutectic microstructure as a function of aging at 330 °C.

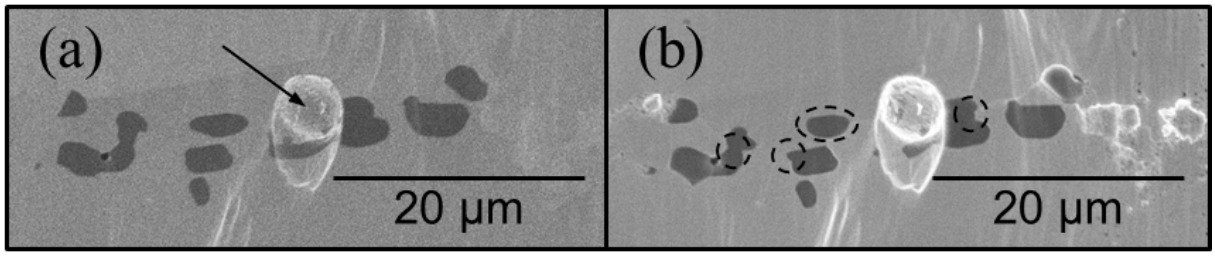

Fig. 16. SEM micrographs of the same cross-section (⊥-plane) of one annealed sample. (a) Shows a fresh cross-section taken after 52 hours at 330 °C. (b) Shows how the same section evolved after another 18 hours at 330 °C in a vacuum. A slight geometrical change is visible for the Ge domains (dark) marked with a dashed line. A spherical void (quiver) is visible at the center of the images.

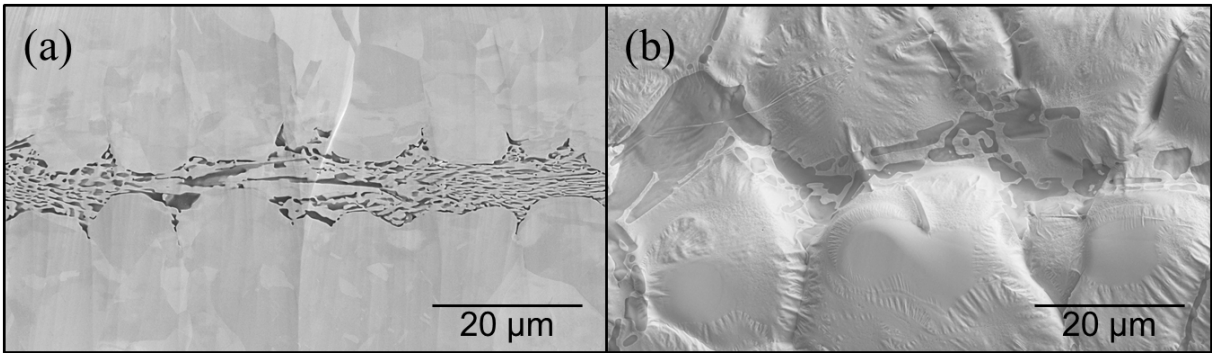

Fig. 17. SEM micrographs of a cross-section (⊥-plane) before (a) and after (b) exposure to 380 °C. The sample was exposed to a temperature above the eutectic melting point (361 °C) for about 20 min. The microstructure was transformed into a coarsened structure. The surface shows clear signs of a melting process. The fine lamellae structure seen in (a) has been transformed into large explicit Ge domains after melting (b). The Ge domains are found in grain boundaries between Au grains protruding away (up and down) from the original bond line (horizontal mid-plane).

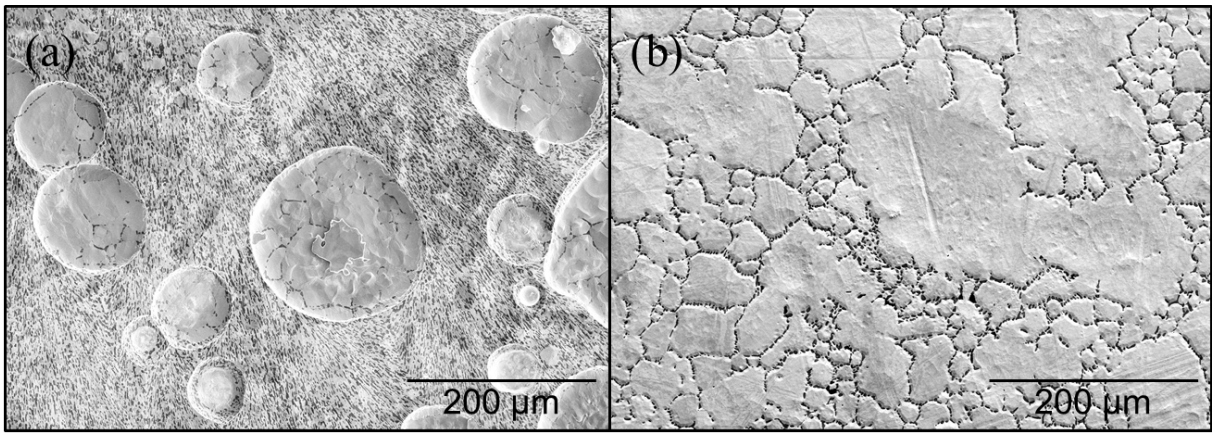

Fig. 18. SEM micrographs of two different ‖-plane cross-sections from the same sample with a slight offset to each other. (a) Shows a near mid-plane section of the bond line, *i.e.,* in the middle of the Au–Ge band, equivalent to L_0 in Fig. 6(a). Round Au structures surrounded by a Ge-rich eutectic Au–Ge mixture. (b) Shows a section 5–10 µm offset from the center of the joint, equivalent to L_1 in Fig. 6(a). Ge domains are visible as a band of pearls along the grain boundaries between Au grains. The sample was annealed for 28 hours at 330 °C.

IV. CONCLUSIONS

Analysis of Au-rich off-eutectic Au–Ge joints formed by a layered Au / eutectic Au–Ge / Au structure revealed an inhomogeneous layered microstructure. Columnar-like structures of primary α-phase (Au) protruded through a Ge rich (28–50 at.% Ge) off-eutectic Au–Ge mixture at the center of the joint (original bond line). In this way, a fraction of the bond area will consist of the primary α-phase (Au). This explains the high-temperature shear strength capacity at 410 °C we report in another publication and demonstrates the suitability of our Au–Ge bonding technique for high-temperature applications[20]. Annealing at high temperature coarsened the microstructure, and Ge diffused and accumulated along grain boundaries between Au grains. When the joints were partially melted, the Ge rapidly diffused and accumulated in larger pure Ge domains surrounded by a Au matrix.

V. ACKNOWLEDGMENT

The authors would like to acknowledge Christian Thoresen (USN). The authors would also like to acknowledge Torleif A. Tollefsen (TEGma AS) and Ole Martin Løvvik (SINTEF) for their support in the project. We would like to thank TECHNI AS, TEGma AS and The Norwegian Research Council for financial support of the project (Project No.: 244915).

VI. REFERENCES

1 V.R. Manikam and K.Y. Cheong: *Components, Packag. Manuf. Technol. IEEE Trans.*, 2011, vol. 1, pp. 457–478.

2 F. Roccaforte, P. Fiorenza, G. Greco, R. Lo Nigro, F. Giannazzo, F. Iucolano, M. Saggio, R. Lo, F. Giannazzo, F. Iucolano, and M. Saggio: *Microelectron. Eng.*, 2018, vol. 187–188, pp. 66–77.

3 W.D. MacDonald and T.W. Eagar: *Annu. Rev. Mater. Sci.*, 1992, vol. 22, pp. 23–46.

4 W.D. MacDonald and T.W. Eagar: *Met. Sci. Join.*, 1992, pp. 93–100.

5 W.D. MacDonald and T.W. Eagar: *Metall. Mater. Trans. A*, 1998, vol. 29A, pp. 315–25.

6 W.F. Gale and D.A. Butts: *Sci. Technol. Weld. Join.*, 2004, vol. 9, pp. 283–300.

7 G.O. Cook and C.D. Sorensen: *J. Mater. Sci.*, 2011, vol. 46, pp. 5305–23.

8 L. Bernstein: *J. Electrochem. Soc.*, 1966, vol. 113, pp. 1282–9.

9 L. Bernstein and H. Bartholomew: *Trans. Metall. Soc. Aime*, 1966, vol. 236, pp. 405–12.

10 H. Liu, K. Wang, K.E. Aasmundtveit, and N. Hoivik: *J. Electron. Mater.*, 2012, vol. 41, pp. 2453–62.

11 K.S. Siow: *J. Electron. Mater.*, 2014, vol. 43, pp. 947–61.

12 F. Yu, J. Cui, Z. Zhou, K. Fang, R.W. Johnson, and M.C. Hamilton: *IEEE Trans. Power Electron.*, 2017,

vol. 32, pp. 7083–95.

13 S.A. Paknejad and S.H. Mannan: *Microelectron. Reliab.*, 2017, vol. 70, pp. 1–11.

14 V. Chidambaram, H.B. Yeung, and G. Shan: *J. Electron. Mater.*, 2012, vol. 41, pp. 2107–17.

15 A. Drevin-Bazin, F. Lacroix, and J.F. Barbot: *J. Electron. Mater.*, 2014, vol. 43, pp. 695–701.

16 S. Tanimoto, K. Matsui, Y. Murakami, H. Yamaguchi, and H. Okumura: in *IMAPS Int. Conf. High Temp. Election. (HiTEC)*, IMAPS, Albuquerque, NM, USA, 2010.

17 H. Okamoto and T.B. Massalski: *Bull. Alloy Phase Diagrams*, 1983, vol. 4, pp. 190–8.

18 H. Okamoto and T.B. Massalski: *Bull. Alloy Phase Diagrams*, 1984, vol. 5, pp. 601–10.

19 H. Okamoto: *J. Phase Equilibria Diffus.*, 2004, vol. 25, pp. 197–8.

20 A. Larsson, T.A. Tollefsen, and K.E. Aasmundtveit: *Microelectron. Reliab.*, 2019, vol. 99, pp. 31–43.

21 A. Larsson, T.A. Tollefsen, O.M. Løvvik, and K.E. Aasmundtveit: in *Eur. Microelectron. Packag. Conf. (EMPC)*, IMAPS, Warsaw, 2017.

22 A. Larsson, C.B. Thoresen, and T. Aamli: in *Proc. Tech. Program - Pan Pac. Microelectron. Symp. (Pan Pacific)*, IEEE, Kauai, HI, USA, 2019.

23 A. Larsson and C.B. Thoresen: *IEEE Trans. Components, Packag. Manuf. Technol.*, 2019, p. 11.

24 R.M. Waghorne, V.G. Rivlin, and G.I. Williams: *J. Phys. F Met. Phys.*, 1976, vol. 6, pp. 147–56.

25 R.P. Elliott and F.A. Shunk: *Bull. Alloy Phase Diagrams*, 1980, vol. 1, pp. 51–4.

26 J. Wang, C. Leinenbach, and M. Roth: *J. Alloy. Compd.*, 2009, vol. 481, pp. 830–6.

27 *MIL-STD-883H*, 2010.

28 F.C. Campbell: *Elements of Metallurgy and Engineering Alloys*, ASM International, USA, 2008.

29 R.J.D. Tilley: *Understanding Solids : The Science of Materials*, John Wiley & Sons, Inc., Chichester, UK, 2004.

30 H. Okamoto: *Desk Handbook: Phase Diagrams for Binary Alloys*, 2nd edn., ASM International, United States of America, 2010.

31 G. Humpston and D.M. Jacobson: *Principles of Soldering*, ASM International, USA, 2004.

32 J.D. Verhoeven: *Fundamentals of Physical Metallurgy*, John Wiley & Sons, Inc., 1975, pp. 169-215.

33 M.E. Glicksman: *Principles of Solidification*, Springer, 2011, pp. 10.1007/978-1-4419-7344-3.